Rashba-type spin splitting at Au(111) beyond the Fermi level: the other part of the story

2013 New J. Phys. 15 105001

(http://iopscience.iop.org/1367-2630/15/10/105001)

New Journal of Physics
The open access journal for physics

Rashba-type spin splitting at Au(111) beyond the Fermi level: the other part of the story

S N P Wissing[1,3], C Eibl[1], A Zumbülte[1], A B Schmidt[1], J Braun[2], J Minár[2], H Ebert[2] and M Donath[1]

[1] Physikalisches Institut, Westfälische Wilhelms-Universität Münster, Wilhelm-Klemm-Straße 10, D-48149 Münster, Germany
[2] Department Chemie, Ludwig-Maximilians-Universität München, Butenandtstraße 11, D-81377 München, Germany
E-mail: Sune.Wissing@uni-muenster.de

New Journal of Physics **15** (2013) 105001 (14pp)
Received 20 June 2013
Published 2 October 2013
Online at http://www.njp.org/
doi:10.1088/1367-2630/15/10/105001

Abstract. We present a combined experimental and theoretical study of spin–orbit-induced spin splittings in the unoccupied surface electronic structure of the prototypical Rashba system Au(111). Spin- and angle-resolved inverse-photoemission measurements reveal a Rashba-type spin splitting in the unoccupied part of the L-gap surface state. With increasing momentum parallel to the surface, the spectral intensity is lowered and the spin splitting vanishes as the surface state approaches the band-gap boundary. Furthermore, we observe significantly spin-dependent peak positions and intensities for transitions between unoccupied sp-like bulk bands. Possible reasons for this behavior are considered: initial and final-state effects as well as the transition itself, which is controlled by selection rules depending on the symmetry of the involved states. Based on model calculations, we identify the initial states as origin of the observed Rashba-type spin effects in bulk transitions.

[3] Author to whom any correspondence should be addressed.

Contents

1. Introduction

The discovery of a spin–orbit-induced spin splitting of the Au(111) Shockley surface state [1] was the starting point of rapidly increasing research on spin-dependent surface electronic states of high-Z materials. Due to their potential applications (e.g. [2, 3]), materials with a spin-dependent electronic bandstructure, especially at surfaces, are interesting candidates for spintronic applications. This is in particular true if the spin separation is based on effects different from magnetic exchange interaction. Spin–orbit interaction can cause spin splittings at the surface of non-magnetic materials by lifting the Kramers degeneracy owing to the lack of inversion symmetry. This effect, known as Rashba–Bychkov [4] splitting, was identified as the origin of the spin splitting of the Au(111) surface state, which was detected by angle-resolved photoemission, first without [1, 5] and later with spin resolution [6]. Since then, many different systems have been investigated for a better understanding of Rashba-type phenomena (e.g. metal surfaces [5, 7, 8] or adsorbate systems [9–14]). Recently, Rashba-type spin polarization was also observed for bulk-derived states within the surface region [15].

So far, experimental information on Rashba-split electronic states has been mainly gained by spin- and angle-resolved photoemission, which provides access to the occupied states. The (111) surfaces of several fcc noble and transition metals exhibit an L-gap surface state with free-electron-like dispersion at the center of the surface Brillouin zone. While typically the lower part of the surface state is occupied and lies within a gap of the projected bulk bandstructure, the unoccupied part approaches the gap boundary, deviates from the parabolic dispersion and becomes a surface resonance. This has been observed for Au(111) [16, 17], Ag(111) [18, 19], Cu(111) [20–24] and Ni(111) [25–28]. Only for the heavy element Au, a sizable spin splitting was observed in the occupied part [6, 29]. No spin-resolved measurements of unoccupied states of the prototypical Au(111) surface have been reported to date.

In this paper, we present spin- and angle-resolved inverse photoemission (IPE) data of Rashba-type splittings in surface and bulk states on Au(111). The experimental work is complemented by *ab initio* calculations of the IPE signal based on the one-step model of photoemission. We follow the unoccupied Rashba-split surface state at higher momentum values as it disperses within the surface projected L-gap, from crossing the Fermi level to hybridizing with bulk states upon approaching the band-gap edge. Furthermore, we present measurements

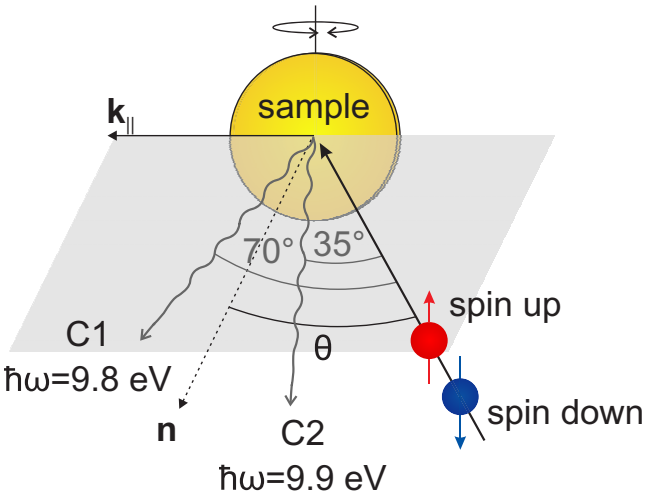

Figure 1. Sketch of the experimental setup. The spin-up (spin-down) direction of the incident electrons, the in-plane wave vector $\mathbf{k}_{\parallel}$ and the surface normal $\mathbf{n}$ form a right-handed (left-handed) coordinate system. Positive (negative) angles of electron incidence θ are realized by rotating the sample toward (away from) the counters. The photons emitted during the IPE process are detected using two Geiger–Müller counters with slightly different photon detection energies and different photon-take-off angles.

of a Rashba-type spin polarization for transitions in sp-like unoccupied bulk states. We discuss the origin of the observed spin polarization and, based on model calculations, attribute it to an initial-state effect.

2. Experiment

2.1. Technique and sample preparation

Spin- and angle-resolved IPE is used to investigate the energy versus momentum dispersion as well as the spin structure of the electronic states above the Fermi level [30]. For excitation, a beam of low-energy electrons with defined energy, momentum and spin from a GaAs photocathode is directed onto the surface. In our setup, its spin polarization P amounts to 33% and its angular divergence to $\Delta\theta = \pm 3.2^{\circ}$. The angular resolution determines the momentum resolution, yet by taking into account the photon energy and the final-state energy. In our case, where we use small photon energies below 10 eV, this corresponds to a resolution of the wave vector parallel to the surface at the Fermi level, i.e. the Fermi momentum, of $\Delta\mathbf{k}_{\parallel,\mathrm{F}} = \pm 0.06\,\text{Å}^{-1}$. Compared with our original experimental setup [31], the electron source has been rotated by 90° to be sensitive to the Rashba spin component. The spin-up (spin-down) direction of the incident electrons, their in-plane wave vector $\mathbf{k}_{\parallel}$ and the surface normal $\mathbf{n}$ form a right-handed (left-handed) coordinate system as shown in figure 1.

The photons emitted during the IPE process are detected by two energy-selective Geiger–Müller counters [32]. Their energy selectivity is based on the ionization threshold of acetone used as counting gas and the transmission cut-off of a CaF_2 entrance window,

whose combination results in an energy bandpass. By heating the entrance window, the cut-off is shifted to lower energies, which results in an improved energy resolution and a shift of the mean detection energy. In our study, we use two counters (cf figure 1): counters C1 and C2 at fixed angles of 70° and 35° with respect to the incident electron beam are operated with window temperatures of $T_{CaF_2} = 370$ and 300 K resulting in pass energies of $\hbar\omega = 9.8$ and 9.9 eV, respectively. The overall energy resolution (FWHM = full width at half maximum) of the experiment, including the energy spread of the incident electron beam, is $\Delta E = 390$ meV for C1 ($\hbar\omega = 9.8$ eV) and $\Delta E = 490$ meV for C2 ($\hbar\omega = 9.9$ eV). Positive (negative) angles of electron incidence θ are realized by rotating the sample toward (away from) the counters.

The Au(111) sample was cleaned by several cycles of sputtering and annealing and its surface quality was verified by low-energy electron diffraction (LEED) and Auger electron spectroscopy. The LEED pattern (not shown) contains additional spots resulting from the $(\sqrt{3} \times 22)$ herringbone reconstruction [33, 34], which is characteristic of the clean Au(111) surface. Unlike in the $\overline{\Gamma}\,\overline{K}$ direction within the surface Brillouin zone, no influence of the herringbone reconstruction on the Au(111) surface state is observed in the $\overline{\Gamma}\,\overline{M}$ and $\overline{\Gamma}\,\overline{M}'$ directions [35, 36]. Therefore, the spectra shown in this paper were obtained along the latter directions. The sample was kept at room temperature during all measurements.

2.2. *Inverse-photoemission results and discussion*

Figure 2 shows a series of spin-resolved IPE spectra for different angles of electron incidence θ taken with counter C1 at a photon detection energy of $\hbar\omega = 9.8$ eV. The filled red pointing-up and blue pointing-down triangles indicate the measured data for the different spin directions spin up and spin down, respectively. The solid lines connecting the data points serve as guides to the eye. All spectra have been normalized to 100% spin polarization of the incident electron beam [37]. The left-hand panel I displays spectra for small angles θ, corresponding to $\mathbf{k}_\parallel$ values around the center of the surface Brillouin zone $\overline{\Gamma}$. Panels II and III show spectra for larger angles up to $\theta = 66°$, reaching $\mathbf{k}_\parallel$ values almost at the zone boundary $\overline{M}'$.

The measured peak positions obtained from the spectra have been summarized in an $E(\mathbf{k}_\parallel)$ plot shown in figure 3. The surface-projected bulk bandstructure [17] is included as gray-shaded area. Figure 3 contains additional data as open triangles, which are extracted from spin-resolved IPE spectra taken with counter C2 at a slightly different detection energy of $\hbar\omega = 9.9$ eV. The solid lines are parabolic fits to the surface-state dispersion measured with angle-resolved photoemission below the Fermi energy E_F [1] with an extrapolation to energies above E_F.

We will discuss our results in three steps: firstly the spectra in the vicinity of $\overline{\Gamma}$, secondly the $E(\mathbf{k}_\parallel)$ region, where the surface state deviates from the parabolic dispersion and approaches the gap boundary and thirdly the spectra for higher θ, where they are dominated by transitions into sp-derived bulk states.

(I) According to photoemission measurements (e.g. [1]), the Shockley surface state SS on Au(111) has its band bottom at 417 meV below E_F close to the center of the surface Brillouin zone $\overline{\Gamma}$. It crosses the Fermi level at $k^{\downarrow}_{\parallel,F} = 0.153\ \text{Å}^{-1}$ and $k^{\uparrow}_{\parallel,F} = 0.176\ \text{Å}^{-1}$. For our photon energies, these wave vectors correspond to an angle of electron incidence of $\theta \approx 8°$. As a consequence, IPE data for normal electron incidence should not show any surface-state intensity. Although the surface-state energy is below E_F for $|\theta| < 8°$, the spectra exhibit small intensity above the Fermi level. This is a consequence of the limited momentum resolution in combination with the temperature-dependent Fermi distribution, the finite lifetime of the surface

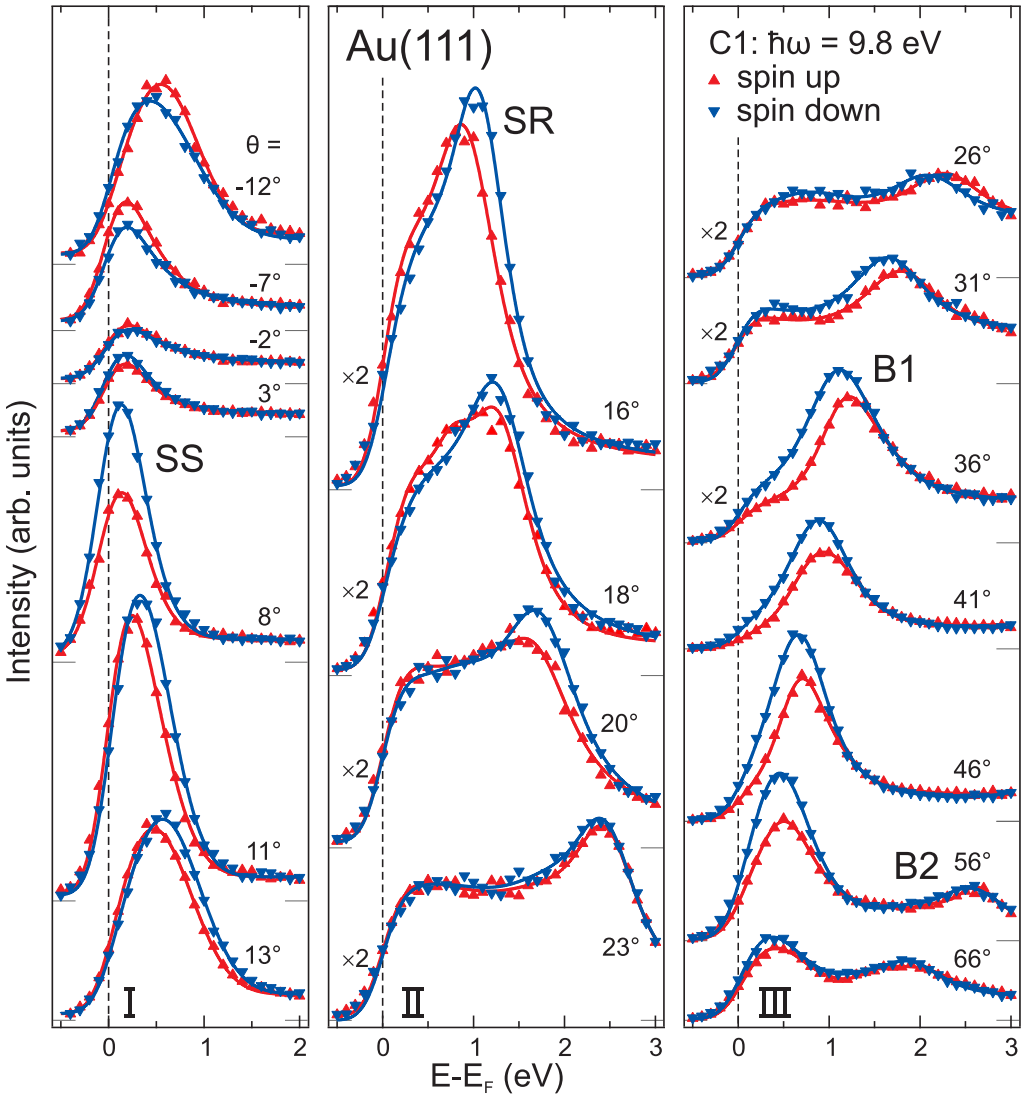

Figure 2. Series of spin-resolved IPE spectra for various angles of electron incidence θ measured with counter C1 at a photon detection energy of $\hbar\omega = 9.8\,\text{eV}$. The data points are shown as filled triangles (red, pointing up for spin up; blue, pointing down for spin down), the solid lines connecting the data points serve as guides to the eye. The three panels I–III cover different regions of θ, which correspond to different $\mathbf{k}_\parallel$ regions as indicated in the $E(\mathbf{k}_\parallel)$ plot in figure 3.

state, and the energy broadening by the apparatus function. This effect has been thoroughly analyzed in the literature for a number of cases [38–40]. Basically, observed spectral peak positions close to the Fermi level do not necessarily coincide with final-state energies in cases where the spectral features appear closer to the Fermi level than the experimental energy resolution. The spectral features never touch the Fermi level but keep away by about half of the energy resolution ΔE.

For $\theta = 8^\circ$ and -7°, high intensity appears right above the Fermi edge. For these angles, the surface state approaches E_F. The spin splitting of the surface state leads to an intensity

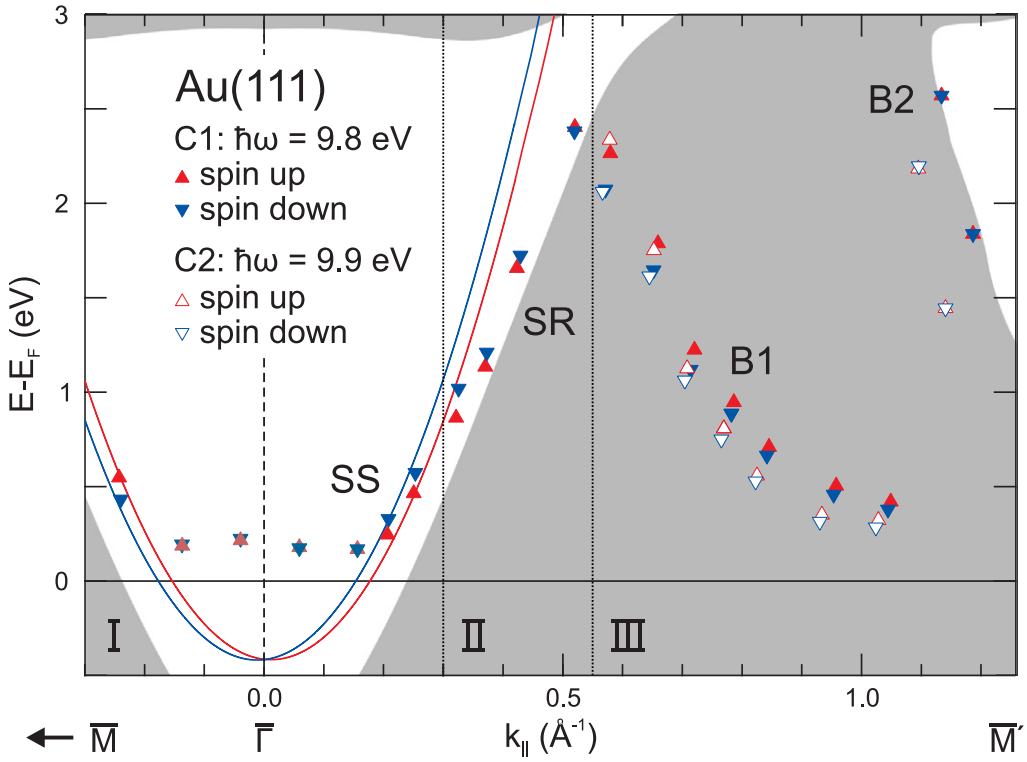

Figure 3. Energy versus $\mathbf{k}_{\parallel}$ dispersion of the unoccupied electronic states of Au(111) along the $\overline{\Gamma}\,\overline{M}$, $\overline{\Gamma}\,\overline{M}'$ directions. The gray-shaded area represents the surface-projected bulk-band structure taken from [17]. The filled and open triangles are derived from measurements with counter C1 ($\hbar\omega = 9.8\,\mathrm{eV}$, cf figure 2) and C2 ($\hbar\omega = 9.9\,\mathrm{eV}$), respectively. The solid lines are parabolic fits to the surface-state dispersion measured with angle-resolved photoemission below the Fermi energy E_F [1] with an extrapolation to energies above E_F.

difference between spin up and spin down because one spin component is closer to E_F than the other. The spin-dependent excess intensity reverses its sign with the sign of the incidence angle. This effect can already be seen for $\theta = 3^\circ$ and -2°. As soon as both spin components of the surface state become unoccupied ($|\theta| > 8^\circ$), the IPE spectra show a feature with a clear Rashba splitting but no longer a strong difference in intensity for the two spin components. The detected spin-dependent energies agree nicely with the parabolic behavior extrapolated from the photoemission data. A comparison of the spectra at $\theta = 11^\circ$, 13° with the spectrum at $\theta = -12^\circ$ illustrates the reversal of the spin splitting as expected. The results so far complement the spin-resolved photoemission results for the occupied part of SS [6]. Finally, it should be noted that the overall spectral intensity differs between spectra for positive and negative angles. This is a consequence of the non-equivalent photon-detection angles in both cases (cf figure 1). It is comparable to the situation in photoemission experiments, where the light used for excitation shines from a certain direction different from the surface normal onto the sample.

(II) The IPE spectra taken at higher angles of incidence between 16° and 20° (cf figure 2(II)) still show a feature with clear Rashba splitting, which continues its dispersion to higher energies (cf figure 3(II)). However, the dispersion starts to deviate from the parabolic

behavior upon approaching the band-gap boundary. Such a deviation from a parabolic dispersion close to the band gap edge is typical for many fcc(111) surface states as mentioned above and can be attributed to an enhanced hybridization of the surface state with bulk states. As a consequence, the spectral weight is shifted deeper into the crystal, the surface-state intensity is reduced, and the line width is broadened. The latter is more pronounced for the spin-up component, which is closer to the band-gap boundary. The surface state is transformed into a surface resonance, therefore labeled SR. Our spin-resolved results show clearly that the described scenario also leads to a reduced spin splitting. This can be understood as a consequence of the decreasing influence of the surface-potential gradient, as the weight of the wave function is reduced in the vicinity of the surface. For $\theta = 23^\circ$, the situation has changed. The spectral feature at about 2.4 eV shows almost no spin dependence, neither in intensity nor in energy. A closer look at the band-gap situation tells us that the state is now well separated from the surface-state parabola and appears close to the bulk regime. We mention as a side note that the spin-dependent background at the low-energy side of the SR structures in figure 2(II) results from indirect transitions between bulk-derived states.

(III) The discovery of a Rashba-type spin polarization in occupied bulk continuum states [15] motivates measurements within the bulk regime of the surface-projected band structure. Calculations for the occupied d-derived states at Au(111) predict spin effects in bulk continuum states within the outermost layers, where photoemission techniques are most sensitive to [41]. No predictions are available for unoccupied states, in particular not for states with sp character. A literature study reveals that early IPE studies on a similar surface, Ag(111) [18, 19, 42], find indications for transitions into sp-derived bulk states in the respective $E(\mathbf{k}_\parallel)$ range. They have been modeled as transitions within the empty-lattice model involving low-index reciprocal lattice vectors $\mathbf{G}$. Due to the free-electron-like character of the involved bands, these transitions appear with rather strong intensity.

These predictions and findings are reason enough to test the spin dependence of transitions into sp-like bulk bands of Au(111). Our IPE data in figure 2(III) for angles θ from 26° to 66° show two spectral features B1 and B2 with $E(\mathbf{k}_\parallel)$ values within the bulk regime (cf figure 3(III)). B1 shows a downward dispersion as $\mathbf{k}_\parallel$ increases. The dispersion behavior is in line with the observations on Ag(111) discussed above. As a surprise, the transition B1 shows a clear spin dependence, yet with reversed splitting compared with the surface-state splitting. With increasing $\mathbf{k}_\parallel$, the spin splitting becomes smaller but the spectra show substantial spin-dependent intensities. The second feature B2 disperses to lower energies as well but it shows neither a Rashba-type splitting nor a spin-dependent difference in the intensity.

In order to gain additional information about the character of the observed states, we compared spectra obtained with counters C1 and C2. They differ with respect to photon energy as well as photon take-off angle. Figure 4 shows spectra for two different electron incidence angles $\theta = 11^\circ$ (upper part, probing SS) and $\theta = 56^\circ$ (lower part, probing B1 and B2). The filled triangles are data taken with C1 at $\hbar\omega = 9.8$ eV and the open triangles are data taken with C2 at $\hbar\omega = 9.9$ eV. Since the early days of photoemission, the photon energy dependence was taken as one criterion for a surface state [43–45]. The energetic position of a surface state should not shift with photon energy because it only depends on $\mathbf{k}_\parallel$ but not on $\mathbf{k}_\perp$, which varies with the photon energy. In contrast, transitions between bulk-derived states depend on the photon energy. From the spectra for $\theta = 11^\circ$ in the upper part of figure 4 it becomes clear that the energetic position of SS is not influenced by the photon energy—as it is expected for a surface

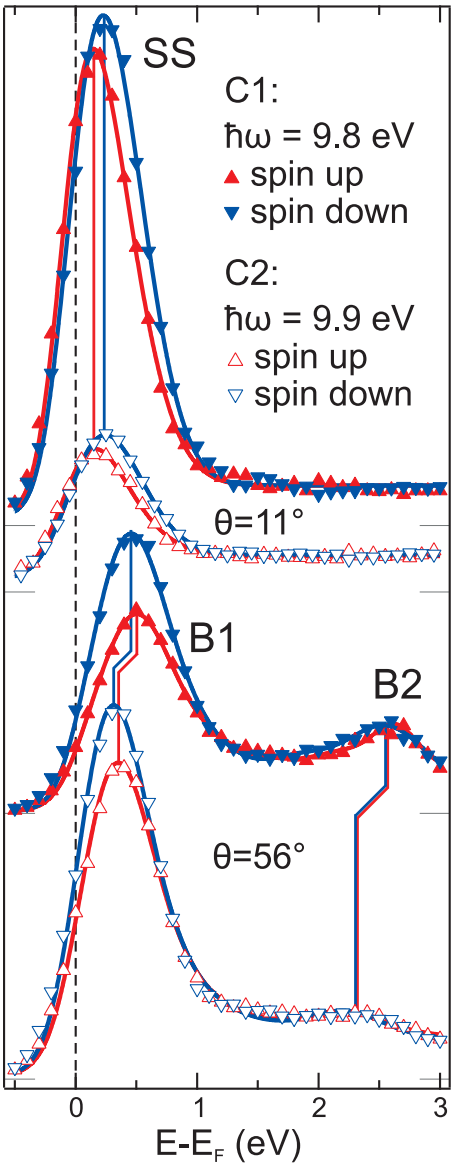

Figure 4. Spin-resolved IPE spectra for two electron incidence angles, taken with counters C1 (filled triangles) and C2 (open triangles) at different detection energies and for different photon take-off angles. The spectra for $\theta = 11^\circ$ (upper part) show the surface-state feature SS. It appears at the same energy for both photon detection energies, yet with different intensity. The spectra for $\theta = 56^\circ$ (lower part) exhibit the bulk transitions B1 and B2. Their energetic positions as well as their intensities change with changing photon energy. The non-changing and changing final-state energy with changing photon energy supports the identification of the respective states as surface and bulk derived, respectively.

state. The different intensities reflect the photon emission characteristics. For the given electron-incidence angle $\theta = 11^\circ$, the photon detection angle is about 60° for C1, while it is about 25° for C2. This emission behavior confirms the expected z-dipole characteristics of the surface-state emission. In contrast, the spectral features B1 and B2, visible in the spectra for $\theta = 56^\circ$ in the

lower part of figure 4, change their energy position with changing photon energy. This behavior was observed for all electron incidence angles, as seen in figure 3. Therefore, we identify B1 and B2 as bulk-derived transitions. This is in line with the observations on Ag(111).

As mentioned above, the Rashba–Bychkov splitting is attributed to the lack of inversion symmetry at the crystal surface. For a closer understanding of the origin of the observed splitting in bulk states, we will refer to the local depth-resolved $\mathbf{k}_{\parallel}$ projected spin density of Au(111) published by Krasovskii and Chulkov [41]. As expected, the average spin polarization over a unit cell is zero within the bulk. At the surface (three outermost atomic layers), however, a large net polarization was found. This polarization of the first atomic layers can be attributed to the interaction of bulk Bloch-waves incident on and reflected from the surface [15, 46]. The Rashba splitting of the surface states leads to a spin dependence of the reflected Bloch waves and therefore induces a polarization to the bulk. As IPE is a surface sensitive method, the Rashba-like splitting observed in our data could be a consequence of the surface sensitivity of the experimental method. A closer look into the theoretical results shows, however, that the theoretically predicted spin effects only appear within the d-like bands. This is a hint that the observed splitting of the transitions into sp-like bulk states is not a final-state effect. It may, therefore, be caused by the initial states and/or by the IPE process itself, i.e. the transition process, which is governed by selection rules depending on the symmetry of the involved states. Please note, an initial-state effect in IPE is equivalent to a final-state effect in photoemission. To get a deeper insight we present a thorough theoretical analysis in the following.

3. Theory

3.1. Computational details

Self-consistent electronic structure calculations were performed within the *ab initio* framework of spin-density functional theory by use of the Vosko *et al* [47] parameterization of the exchange and correlation potential. The electronic structure was calculated within the relativistic multiple-scattering or Korringa–Kohn–Rostoker (KKR) formalism in the tight binding-KKR mode [48–50]. The resulting half-space electronic structure for the Au(111) surface represented by single-site scattering matrices for the different Au atoms and the corresponding wave functions for initial- and final-state energies were used as input quantities for the spectroscopic analysis. For the IPE calculations, performed within the one-step formalism [51–53], an additional layer was placed on top of the first atomic Au layer. This layer represents a Rundgren-type surface potential [54, 55]. To account for, among others, impurity scattering a small constant imaginary value of $V_{\mathrm{i}} = 0.05\,\mathrm{eV}$ was used for the initial state. For the final state a constant imaginary value of $V_{\mathrm{i}} = 2.0\,\mathrm{eV}$ has been chosen again in a phenomenological way. Also, we have renormalized the Fermi level by a rigid energy shift of 0.3 eV to account for a well known shortcoming of the local-density approximation (LDA). Using the LDA one systematically underestimates self-energy effects in the electronic structure of simple metals [56].

As a novel approach, we performed spectral-function as well as IPE calculations using a scheme that allows one to decompose the spin–orbit coupling operator $\hat{\xi} = \boldsymbol{\sigma} \cdot \mathbf{l}$, which appears in the radial Dirac equation, into two different contributions $\hat{\xi} = \boldsymbol{\sigma} \cdot \mathbf{l} = \sigma_z l_z + (\sigma_x l_x + \sigma_y l_y) = \hat{\xi}_{zz} + \hat{\xi}_{xy}$ [57]. The first of the two terms of this formalism lifts energetic degeneracies but leaves the spin as a good quantum number, while the second causes hybridization of states

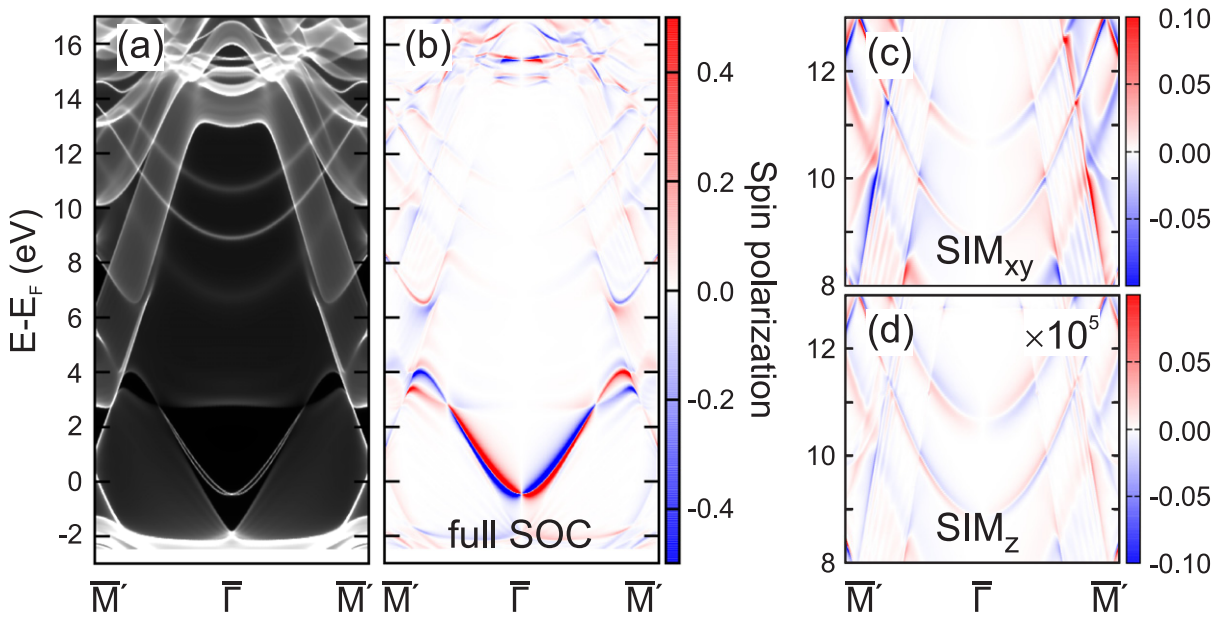

Figure 5. (a) Bloch spectral function calculated for the Au(111) surface along the $\overline{\Gamma}\,\overline{M}'$ direction. The unoccupied electronic structure including the Rashba-split surface state, which disperses around the Fermi level, is shown. High spectral intensity is indicated by white color. (b) Spin-projected spectral function representing the Rashba component of the spin polarization. Red (blue) color indicates spin-up (spin-down) states. (c) Calculated Rashba component using only the part of the spin–orbit interaction that causes hybridization of states with different spin character. (d) Same type of calculation but accounting for the spin-conserving part of the spin–orbit interaction only.

with different spin character. If one chooses a surface fixed coordinate system with the z-axis being the surface normal and uses only the first term $\hat{\xi}_{zz}$ for an electronic structure simulation (SIM$_z$), one would expect non-zero spin polarization only in the z-component, due to the spin-conserving nature of the remaining Hamiltonian [57]. Performing a simulation by use of the Pauli matrices σ_x and σ_y only (SIM$_{xy}$), a corresponding in-plane or Rashba-type polarization should appear with values that are comparable to those one would expect in a full simulation (full SOC). We show in the next section that this method permits a detailed analysis on the origin of Rashba-type splittings observed by our measurements of transitions between unoccupied bulk states of Au(111).

3.2. Unoccupied electronic structure of Au(111)

First we discuss the electronic structure of the Au(111) surface in terms of the spectral function calculated for the complete semi-infinite half space. In figure 5(a) the spectral function is shown along the $\overline{\Gamma}\,\overline{M}'$ direction. All energy scales refer to $E_F = 0$. Inspecting first the energy region around the Fermi level the Rashba-split surface state is clearly visible. The value of the Rashba parameter α_R [55] which is a measure of the splitting in $\mathbf{k}_\parallel$ amounts to 0.37 eV Å. This is in good agreement with previous experimental results [1, 55]. The surface state disperses in the vicinity

of the projected bulk-band structure and enters this region with nearly zero spectral weight at about 2 eV above the Fermi level. The unoccupied bulk-band structure is shown up to 17 eV above E_F to include the initial states of the IPE process.

The Rashba component of the spin polarization is shown in figure 5(b). Red (blue) color indicates spin-up (spin-down) states. To visualize the non-zero spin polarization of the higher lying unoccupied bulk states we have reduced the color scale to ±0.5. Nevertheless, the surface state is 100% polarized with a color pattern typical for Rashba-split states. The bulk states at lower energies, however, appear completely unpolarized. This has been checked by a careful analysis of our corresponding theoretical data and is in good agreement with previous theoretical work [41]. A Rashba-type spin polarization is obviously present in the unoccupied bulk states above 6 eV where the influence of higher-lying d bands comes into play. A more detailed analysis of that is shown in figures 5(c) and (d) for the energy region between 8 and 13 eV.

For figure 5(c) we used in the calculation only the part of the spin–orbit interaction that causes hybridization of states with different spin character (SIM_{xy}). A more precise inspection reveals that this calculation is very close to the calculation where the full spin–orbit operator was used. In other words, we find nearly the same result as shown in figure 5(b). Using the spin-conserving part only (SIM_z) the situation is very different (cf figure 5(d)). The Rashba component of the spin polarization is almost zero for the bulk-derived states. Therefore, we conclude that the peculiar Rashba splitting observed in the measurements is caused by the SIM_{xy} part of the spin–orbit interaction and, in consequence, we identify it as an initial-state effect in IPE.

To verify this assumption we additionally performed two types of IPE calculations. The first one, as usual, takes care of the full spin–orbit interaction, within the second one we used the spin-conserving part only. This procedure allows to check the impact of non-spin-conserving processes on (inverse) photoemission of bulk-derived states. The results of these calculations are discussed below.

3.3. One-step calculations

Here, we present our IPE calculations considering matrix-element effects, initial-state effects and the influence of the surface in a quantitative way. Figure 6 shows two series of spin-resolved IPE spectra calculated for the given experimental geometry. Only the unpolarized radiation measured in the experiment was simulated by an incoherent superposition of spectra calculated for outgoing linear s- and p-polarized light. In figure 6(a) we show the angular-dependent series of IPE spectra calculated by use of the full Hamiltonian (full SOC). Comparing these spectra with their experimental counterparts, shown in figure 2(II), we clearly observe both bulk states denoted by B1 and B2. The dispersion behavior of these spectral features is found in good agreement with the experimental findings. Furthermore, the Rashba-type spin splittings, reversed with respect to the splitting of SS, is well reproduced by theory. Only the intensity asymmetries have been overestimated in the calculations, although the trend in the spectral series is qualitatively reproduced. The reason for these deviations is found in terms of matrix-element effects.

Figure 6(b) shows the SIM_z simulation where the calculated IPE spectra are based on the spin-conserving part of the Hamiltonian. At a first glance the dispersion behavior as well as the relative intensities are only qualitatively reproduced. Also the intensity asymmetries have been underestimated in comparison to the experimental data. This seems to be an intrinsic feature

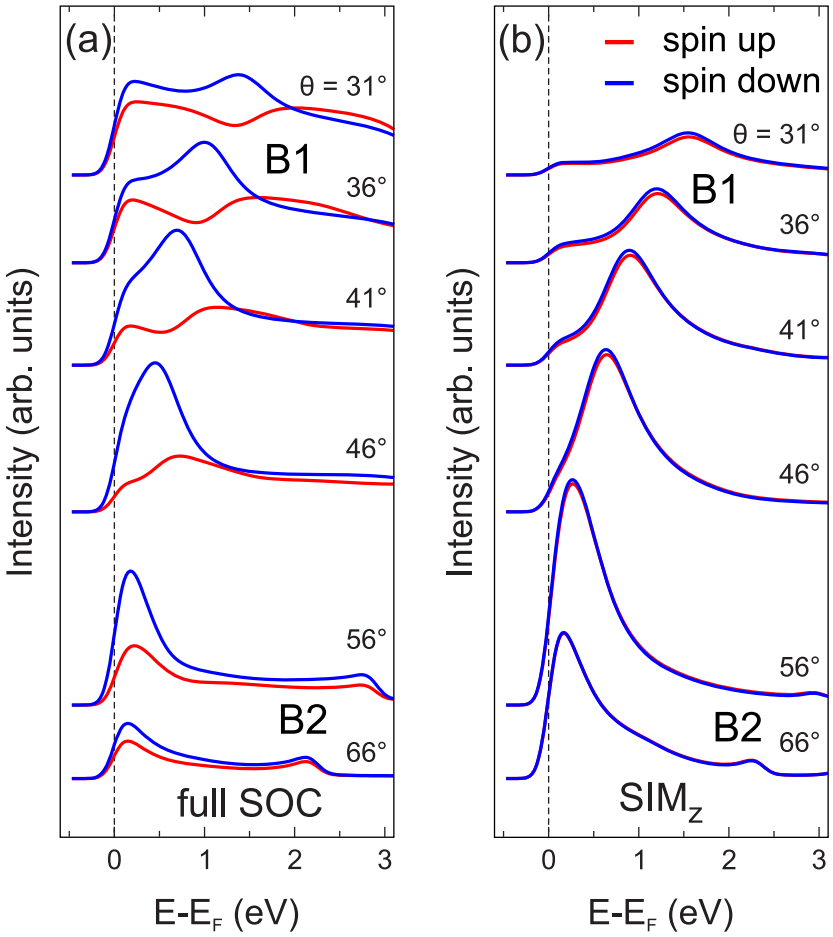

Figure 6. Series of spin-resolved IPE spectra calculated for various angles of electron incidence along the $\overline{\Gamma}\,\overline{M}'$ direction at a fixed photon detection energy of $\hbar\omega = 9.8$ eV. Red (blue) color indicates spin-up (spin-down) states. (a) Full consideration of spin–orbit coupling in the calculations. (b) Only the spin-conserving part of the spin–orbit interaction was accounted for.

of such a simulation [57]. Besides these minor shortcomings the most important observation is the absence of the Rashba-type splitting in the bulk state B1. This proves our assumption which was based on a calculation of the spectral function and unambiguously assign this phenomenon to an initial-state effect caused by a Rashba-type splitting present in the unoccupied bulk states at higher energies.

4. Conclusion

One part of the Au(111) story, i.e. for energies below the Fermi level, was already told in the literature on the basis of spin- and angle-resolved photoemission studies. The other part of the story, for energies above the Fermi level, is given in this paper. We studied the influence of the spin–orbit coupling on the unoccupied surface electronic structure of Au(111). Spin- and angle-resolved IPE as well as calculations within the one-step model of photoemission were

used to identify and describe the spin dependence of surface and bulk states as they disperse along the $\overline{\Gamma}\,\overline{M}$ direction of the surface Brillouin zone. We followed the unoccupied Rashba-split surface state at higher momentum values, from crossing the Fermi level to hybridizing with bulk states upon approaching the band-gap edge, where the spin dependence is lost. Furthermore, we presented measurements of a Rashba-type spin polarization for transitions in sp-like unoccupied bulk states. We discussed possible reasons for this behavior, namely initial- and final-state effects and the transition itself, which is controlled by selection rules depending on the symmetry of the involved states. Based on model calculations, we attributed the observed spin polarization to the spin dependence of the initial states.

Acknowledgments

It is a pleasure to thank J Henk for fruitful discussions and W Mai and H Wensing for excellent technical support. JB, JM and HE gratefully acknowledge financial support from the Deutsche Forschungsgemeinschaft (Projekt SPP 1666, EBE-154/20, EBE-154/23) and the Bundesministerium für Bildung und Forschung through BMBF:05K10WMA. The publication of this work was supported by the Deutsche Forschungsgemeinschaft and the Open Access Publication Fund of the University of Münster.

References

[1] LaShell S, McDougall B A and Jensen E 1996 *Phys. Rev. Lett.* **77** 3419
[2] Datta S and Das B 1990 *Appl. Phys. Lett.* **56** 665
[3] Miron I M *et al* 2011 *Nature Mater.* **10** 419
[4] Bychkov Y A and Rashba E I 1984 *JETP Lett.* **39** 66
[5] Nicolay G, Reinert F, Hüfner S and Blaha P 2001 *Phys. Rev.* B **65** 033407
[6] Hoesch M, Muntwiler M, Petrov V N, Hengsberger M, Patthey L, Shi M, Falub M, Greber T and Osterwalder J 2004 *Phys. Rev.* B **69** 241401
[7] Koroteev Y M, Bihlmayer G, Gayone J E, Chulkov E V, Blügel S, Echenique P M and Hofmann P 2004 *Phys. Rev. Lett.* **93** 046403
[8] Miyamoto K, Kimura A, Okuda T, Shimada K, Iwasawa H, Hayashi H, Namatame H, Taniguchi M and Donath M 2012 *Phys. Rev.* B **86** 161411
[9] Ast C R, Henk J, Ernst A, Moreschini L, Falub M C, Pacile D, Bruno P, Kern K and Grioni M 2007 *Phys. Rev. Lett.* **98** 186807
[10] Gierz I, Suzuki T, Frantzeskakis E, Pons S, Ostanin S, Ernst A, Henk J, Grioni M, Kern K and Ast C R 2009 *Phys. Rev. Lett.* **103** 046803
[11] Meier F, Dil H, Lobo-Checa J, Patthey L and Osterwalder J 2008 *Phys. Rev.* B **77** 165431
[12] Sakamoto K *et al* 2009 *Phys. Rev. Lett.* **102** 096805
[13] Shikin A M, Varykhalov A, Prudnikova G V, Usachov D, Adamchuk V K, Yamada Y, Riley J D and Rader O 2008 *Phys. Rev. Lett.* **100** 057601
[14] Takayama A, Sato T, Souma S and Takahashi T 2011 *Phys. Rev. Lett.* **106** 166401
[15] Kimura A *et al* 2010 *Phys. Rev. Lett.* **105** 076804
[16] Woodruff D P, Royer W A and Smith N V 1986 *Phys. Rev.* B **34** 764
[17] Takeuchi N, Chan C T and Ho K M 1991 *Phys. Rev.* B **43** 13899
[18] Hulbert S L, Johnson P D, Stoffel N G and Smith N V 1985 *Phys. Rev.* B **32** 3451
[19] Altmann W, Dose V and Goldmann A 1986 *Z. Phys.* B **65** 171
[20] Goldmann A, Dose V and Borstel G 1985 *Phys. Rev.* B **32** 1971

[21] Hulbert S L, Johnson P D, Stoffel N G, Royer W A and Smith N V 1985 *Phys. Rev.* B **31** 6815
[22] Jacob W, Dose V, Kolac U, Fauster T and Goldmann A 1986 *Z. Phys.* B **63** 459
[23] Grass M, Braun J, Borstel G, Schneider R, Durr H, Fauster T and Dose V 1993 *J. Phys.: Condens. Matter* **5** 599
[24] Akin Ünal A, Tusche C, Ouazi S, Wedekind S, Chiang C T, Winkelmann A, Sander D, Henk J and Kirschner J 2011 *Phys. Rev.* B **84** 073107
[25] Goldmann A, Donath M, Altmann W and Dose V 1985 *Phys. Rev.* B **32** 837
[26] Borstel G, Thörner G, Donath M, Dose V and Goldmann A 1985 *Solid State Commun.* **55** 469
[27] Braun J and Donath M 2002 *Europhys. Lett.* **59** 592
[28] Braun J and Donath M 2004 *J. Phys.: Condens. Matter* **16** 2539
[29] Henk J, Hoesch M, Osterwalder J, Ernst A and Bruno P 2004 *J. Phys.: Condens. Matter* **16** 7581
[30] Donath M 1999 *J. Phys.: Condens. Matter* **11** 9421
[31] Kolac U, Donath M, Ertl K, Liebl H and Dose V 1988 *Rev. Sci. Instrum.* **59** 1933
[32] Budke M, Renken V, Liebl H, Rangelov G and Donath M 2007 *Rev. Sci. Instrum.* **78** 083903
[33] Perdereau J, Biberian J P and Rhead G E 1974 *J. Phys. F: Met. Phys.* **4** 798
[34] Van Hove M, Koestner R, Stair P, Bibérian J, Kesmodel L, Bartos I and Somorjai G 1981 *Surf. Sci.* **103** 189
[35] Chen W, Madhavan V, Jamneala T and Crommie M F 1998 *Phys. Rev. Lett.* **80** 1469
[36] Reinert F and Nicolay G 2004 *Appl. Phys.* A **78** 817
[37] Donath M 1989 *Appl. Phys.* A **49** 351
[38] Donath M and Dose V 1989 *Europhys. Lett.* **9** 821
[39] Budke M, Allmers T, Donath M and Rangelov G 2007 *Rev. Sci. Instrum.* **78** 113909
[40] Stolwijk S D, Schmidt A B and Donath M 2010 *Phys. Rev.* B **82** 201412
[41] Krasovskii E E and Chulkov E V 2011 *Phys. Rev.* B **83** 155401
[42] Ilver L, Kovacs A, Kanski J, Nilsson P O and Sobczak E 1987 *Phys. Scr.* **35** 726
[43] Gartland P O and Slagsvold B J 1975 *Phys. Rev.* B **12** 4047
[44] Knapp J A, Himpsel F J and Eastman D E 1979 *Phys. Rev.* B **19** 4952
[45] Plummer E W and Eberhardt W 2007 *Advances in Chemical Physics* (New York: Wiley) p 533
[46] Krasovskii E E, Strocov V N, Barrett N, Berger H, Schattke W and Claessen R 2007 *Phys. Rev.* B **75** 045432
[47] Vosko S H, Wilk L and Nusair M 1980 *Can. J. Phys.* **58** 1200
[48] Ebert H 2000 *Electronic Structure and Physical Properties of Solids* (*Lecture Notes in Physics* vol 535) ed H Dreyssé (Berlin: Springer) p 191
[49] Ebert H, Ködderitzsch D and Minár J 2011 *Rep. Prog. Phys.* **74** 096501
[50] Ebert H *et al* 2012 *The Munich SPR-KKR Package* version 6.3 (http://olymp.cup.uni-muenchen.de:/ak/ebert/SPRKKR)
[51] Pendry J 1976 *Surf. Sci.* **57** 679
[52] Hopkinson J, Pendry J and Titterington D 1980 *Comput. Phys. Commun.* **19** 69
[53] Braun J 1996 *Rep. Prog. Phys.* **59** 1267
[54] Malmström G and Rundgren J 1980 *Comput. Phys. Commun.* **19** 263
[55] Nuber A, Braun J, Forster F, Minár J, Reinert F and Ebert H 2011 *Phys. Rev.* B **83** 165401
[56] Eckardt H, Fritsche L and Noffke J 1984 *J. Phys. F: Met. Phys.* **14** 97
[57] Ebert H, Freyer H and Deng M 1997 *Phys. Rev.* B **56** 9454